arXiv:1405.1082v1 [astro-ph.HE] 5 May 2014

Draft Version

A STRONG RADIO BRIGHTENING AT THE JET BASE OF M 87 DURING THE ELEVATED VERY-HIGH-ENERGY GAMMA-RAY STATE IN 2012

K. Hada[1,2], M. Giroletti[1], M. Kino[3,4], G. Giovannini[1,5], F. D'Ammando[1], C. C. Cheung[6], M. Beilicke[7], H. Nagai[8], A. Doi[4], K. Akiyama[2,9], M. Honma[2,10], K. Niinuma[10], C. Casadio[12], M. Orienti[1], H. Krawczynski[7], J. L. Gómez[12], S. Sawada-Satoh[2], S. Koyama[2,4,9], A. Cesarini[13], S. Nakahara[14], M. A. Gurwell[15]

[1]*INAF Istituto di Radioastronomia, via Gobetti 101, I-40129 Bologna, Italy;* hada@ira.inaf.it

[2]*Mizusawa VLBI Observatory, National Astronomical Observatory of Japan, Osawa, Mitaka, Tokyo 181-8588, Japan*

[3]*Korea Astronomy and Space Science Institute (KASI), 776 Daedeokdae-ro, Yuseong-gu, Daejeon 305-348, Republic of Korea*

[4]*Institute of Space and Astronautical Science, Japan Aerospace Exploration Agency, 3-1-1 Yoshinodai, Chuo, Sagamihara 252-5210, Japan*

[5]*Dipartimento di Fisica e Astronomia, Università di Bologna, via Ranzani 1, I-40127 Bologna, Italy*

[6]*Space Science Division, Naval Research Laboratory, Washington, DC 20375, USA*

[7]*Physics Department and McDonnell Center for the Space Sciences, Washington University, St. Louis, MO 63130, USA*

[8]*National Astronomical Observatory of Japan, Osawa, Mitaka, Tokyo 181-8588, Japan*

[9]*Department of Astronomy, Graduate School of Science, The University of Tokyo, 7-3-1 Hongo, Bunkyo-ku, Tokyo 113-0033, Japan*

[10]*Department of Astronomical Science, The Graduate University for Advanced Studies (SOKENDAI), 2-21-1 Osawa, Mitaka, Tokyo 181-8588, Japan*

[11]*Graduate School of Science and Engineering, Yamaguchi University, 1677-1 Yoshida, Yamaguchi, 753-8512, Japan*

[12]*Instituto de Astrofisica de Andalucia, CSIC, Apartado 3004, 18080 Granada, Spain*

[13]*Department of Physics, University of Trento, I38050, Povo, Trento, Italy*

[14]*Faculty of Science, Kagoshima University, 1-21-35 Korimoto, Kagoshima, Kagoshima 890-0065, Japan*

[15]*Harvard-Smithsonian Center for Astrophysics, Cambridge MA 02138 USA*

ABSTRACT

We report our intensive, high-angular-resolution radio monitoring observations of the jet in M 87 with the VLBI Exploration of Radio Astrometry (VERA) and the European VLBI Network (EVN) from February 2011 to October 2012, together with contemporaneous high-energy (HE; 100 MeV$< E <$100 GeV) γ-ray light curves obtained by the *Fermi* Large Area Telescope (LAT). During this period (specifically from February 2012 to March 2012), an elevated level of the M 87 flux is reported at very-high-energy (VHE; $E > 100$ GeV) γ-rays by VERITAS. We detected a remarkable (up to $\sim$70%) increase of the radio flux density from the unresolved jet base (radio core) with VERA at 22 and 43 GHz coincident with the VHE activity. Meanwhile, we confirmed with EVN at 5 GHz that the peculiar knot HST-1, which is an alternative favored γ-ray production site located at $\gtrsim$120 pc from the nucleus, remained quiescent in terms of its flux density and structure. These results in the radio bands strongly suggest that the VHE γ-ray activity in 2012 originates in the jet base within 0.03 pc or 56 Schwarzschild radii (the VERA spatial resolution of 0.4 mas at 43 GHz) from the central supermassive black hole. We further conducted VERA astrometry for the M 87 core at six epochs during the flaring period, and detected core shifts between 22 and 43 GHz, a mean value of which is similar to that measured in the previous astrometric measurements. We also discovered a clear frequency-dependent evolution of the radio core flare at 43, 22 and 5 GHz; the radio flux density increased more rapidly at higher frequencies with a larger amplitude, and the light curves clearly showed a time-lag between the peaks at 22 and 43 GHz, the value of which is constrained to be within $\sim 35 - 124$ days. This indicates that a new radio-emitting component was created near the black hole in the period of the VHE event, and then propagated outward with progressively decreasing synchrotron opacity. By combining the obtained core shift and time-lag, we estimated an apparent speed of the newborn component propagating through the opaque region between the cores at 22 and 43 GHz. We derived a sub-luminal speed (less than $\sim 0.2c$) for this component. This value is significantly slower than the super-luminal ($\sim 1.1c$) features that appeared from the core during the prominent VHE flaring event in 2008, suggesting that the stronger VHE activity can be associated with the production of the higher Lorentz factor jet in M 87.

Subject headings: galaxies: active — galaxies: individual (M 87) — galaxies: jets — gamma rays: galaxies — radio continuum: galaxies

1. Introduction

Active galactic nuclei (AGNs) generate powerful relativistic jets which are thought to be a consequence of the material accretion onto the supermassive black holes. The nearby radio galaxy M 87 accompanies one of the best studied AGN jets, and its proximity ($D = 16.7$ Mpc; Blakeslee et al. 2009) and brightness have enabled intensive studies of this jet over decades from radio, optical and to X-ray at tens of parsec scale resolutions (e.g., Owen et al. 1989; Biretta et al. 1999; Harris et al. 2006). Moreover, the inferred very massive black hole ($M_{\rm BH} \simeq (3-6) \times 10^9\ M_\odot$; Macchetto et al. 1997; Gebhardt & Thomas 2009; Walsh et al. 2013) yields a linear resolution down to 1 milliarcsecond (mas) = 0.08 pc = 140 Schwarzschild radii ($R_{\rm s}$) [1], making this source a unique case to probe the relativistic-jet formation at an unprecedented compact scale with Very-Long-Baseline-Interferometer (VLBI) observations (Junor et al. 1999; Kovalev et al. 2007; Hada et al. 2011; Doeleman et al. 2012; Hada et al. 2013).

With the advent of the new-generation Cherenkov telescope arrays, M 87 is now well known to show γ-ray emission up to the very-high-energy (VHE; $E > 100$ GeV) regime, where this source often exhibits active flaring episodes. The location and the physical processes of such emission have been a matter of debate over the past years. To date, M 87 underwent three remarkable flaring events in 2005, 2008 and 2010. In 2005, a VHE flare (Aharonian et al. 2006) was accompanied by the radio-to-X-ray outbursts from HST-1, a violent knot located at a de-projected distance of $\gtrsim$120 pc downstream of the nucleus (Harris et al. 2006)[2], with the emergence of superluminal ($\sim 4c$) radio features (Cheung et al. 2007). These results led to the argument that HST-1 is associated with the VHE γ-ray production (e.g., Stawarz et al. 2006; Cheung et al. 2007; Harris et al. 2008, 2009). In the case of the 2008 event (Acciari et al. 2009), on the other hand, the *Chandra X-ray Observatory* detected an enhanced X-ray flux from the nucleus, while HST-1 maintained a comparatively constant flux. In addition, the VLBA observations at 43 GHz during the VHE activity detected a strong flux increase from the radio core at the jet base. These facts provide the strong claim that the VHE flare originates in the core (Acciari et al. 2009). The third event occurring in 2010 is rather elusive. Coincident with the VHE event, *Chandra* again detected an enhanced flux from the X-ray core (Harris et al. 2011; Abramowski et al. 2012), and VLBA observations also suggested a possible increase of the radio core flux (Hada et al. 2012). However, Giroletti et al. (2012) found the emergence of a superluminal component in the HST-1 complex

[1] In this paper we adopt $M_{\rm BH} = 6 \times 10^9 M_\odot$ along with Hada et al. (2011, 2012, 2013), although we note that the exact value of $M_{\rm BH}$ in M 87 is still controversial and should be carefully considered. One can rescale the values in $R_{\rm s}$ unit in this paper by multiplying a factor of 2 if $M_{\rm BH} = 3 \times 10^9 M_\odot$ is used.

[2] The exact distance of HST-1 depends on the viewing angle of the M 87 jet i. While Ly et al. (2007) estimates $i \sim 30^\circ - 45^\circ$ based on their sub-parsec radio jet study, the observed superluminal motions of HST-1 up to $6\,c$ (at optical wavelength) suggest a smaller viewing angle close to $i \sim 15^\circ$ (Biretta et al. 1999). The recent optical polarization study of HST-1 also suggests the trend of the smaller viewing angle mentioned above (Perlman et al. 2011). A detailed discussion for the viewing angle of M 87 is given in Acciari et al. (2009), who suggested a likely range to be $i \sim 15^\circ - 25^\circ$ by surveying the literature.

near the epoch of this event, which is reminiscent of the 2005 case.

At high-energy (HE; 100 MeV< E <100 GeV) γ rays, the *Fermi* Large Area Telescope (LAT) detects a faint, point-like γ-ray emission within the central $\sim$20 kpc of the galaxy in 10 months of all-sky survey (Abdo et al. 2009). Contrary to the variable VHE γ-rays, the emission in the MeV/GeV regime appears to be stable (at least) on a timescale of about 10$\sim$30 days, although the same amplitude of fluctuations as in TeV would have been difficult to detect given the lower significance of detection in this band. The observed MeV/GeV spectrum seems to connect smoothly with the VHE spectrum at a low (non-flaring) state (Abdo et al. 2009).

Recently, the VERITAS Collaboration has reported new VHE γ-ray activity from M 87 in early 2012 (Beilicke et al. 2012). While there were no remarkable flares like those in the previous episodes (where the peak fluxes reached $\Phi_{>0.35\mathrm{TeV}}$ $\sim$(1–3)$\times10^{-11}$ photons cm^{-2} s^{-1}; Abramowski et al. 2012), the VHE flux in 2012 clearly exhibits an elevated state at a level of $\sim9\sigma$ ($\Phi_{>0.35\mathrm{TeV}}$ $\sim$(0.2–0.3)$\times10^{-11}$ photons cm^{-2} s^{-1}) over the consecutive two months from February to March 2012. The observed flux is a factor of $\sim$2 brighter than that in the neighboring quiescent periods. To understand the nature and the origin of this event in more detail, it is crucial to explore the contemporaneous status of M 87 in other wavebands, particularly where higher-resolution instruments are available.

Here we report a multi-wavelength radio and MeV/GeV study of the M 87 jet during this period using the VLBI Exploration Radio Astrometry (VERA), the European VLBI Network (EVN), the Submillimeter Array (SMA) and the *Fermi*-LAT. We especially focus on the VLBI data in the radio bands. With VERA, we obtained a high-angular-resolution, phase-referencing data set at 22 and 43 GHz with a dense time interval during the VHE activity in 2012. With the supportive EVN monitoring, we obtained a complementary data set at 5 GHz, which enables a high-sensitivity imaging of the M 87 jet. A collective set of these radio data allows us to probe the detailed physical status and structural evolutions of M 87 by pinpointing the candidate sites of the γ-ray emission i.e., the core and HST-1. In Section 2, we present the radio data analyses for VERA, EVN and SMA. In Section 3, we describe the selection and analysis of the *Fermi*-LAT data. We then describe our results and discussion in Section 4 and 5, respectively. In the final section, we will summarize the paper. In the present paper, the spectral index α is defined as $S_\nu \propto \nu^{+\alpha}$.

2. Radio data: observations and reduction

2.1. VERA dedicated sessions at 22 and 43 GHz (Mode-A)

On 2012 February 24, March 16, 21, April 5, 27 and May 17, we made dedicated observations of M 87 with VERA at 22.3 and 43.1 GHz (hereafter we term these sessions as *Mode-A*). All four of the VERA stations participated in good weather conditions. Left-handed circular polarization was received and sampled with a 2-bit quantization using the VERA digital filter unit. We employed

dual-beam observations to allow astrometric measurements; M 87 and a nearby radio source M 84 (separated by 1.°5 on the sky from M 87) were observed simultaneously. The data were recorded at a rate of 1024 Mbps (a total bandwidth of (128+128) MHz), where each of the two 128 MHz-wide subbands was allocated for each source. In an effort to reduce systematic errors and to achieve similar *uv* coverages between the two frequencies, each frequency was alternated in turn every 80 minutes. At each epoch, the total on-source time results in about 3 hours at each frequency.

The initial data calibration was performed with the Astronomical Image Processing System (AIPS) developed at the National Radio Astronomy Observatory (NRAO). First, a-priori amplitude calibration was applied using the measured system noise temperature and the elevation-gain curve of each antenna. We then calibrated the amplitude part of bandpass characteristics at each station using the auto-correlation data. Next, we employed the calibration of the fringe phases in the following processes; first, we recalculated delay-tracking solutions for the correlated data using an improved delay-tracking model. Throughout the data analysis, we adopt the delay-tracking center as $\alpha_{\rm J2000} = 12^{\rm h}30^{\rm m}49\overset{\rm s}{.}4233830$ and $\delta_{\rm J2000} = 12^\circ23'28\overset{''}{.}043840$ for M 87, while $\alpha_{\rm J2000} = 12^{\rm h}25^{\rm m}03\overset{\rm s}{.}7433330$ and $\delta_{\rm J2000} = 12^\circ53'13\overset{''}{.}139330$ for M 84. The delay-tracking solutions include delay contributions from the atmosphere, which are estimated using the global positioning system data (Honma et al. 2007). Next, we calibrated the differences due to instrumental delays between the two signal paths in the dual beam, which are measured using artificial noise signals injected at the same time into the two receivers (Honma et al. 2008). After that, we performed fringe-fitting to remove residual delays, rates and phases. Because M 87 is much brighter than M 84, we chose M 87 as a phase calibrator and transferred the derived fringe solutions to the data of M 84. A fringe-fitting on M 87 was conducted assuming a point source model. Deviations of the phase/gain solutions from the point source model for M 87 were further corrected using the self-calibrated images, the production process of which is described below. Finally, the corrected phase and gain solutions were applied to M 84 and its phase-referenced images were created, in which the relative position of M 84 with respect to M 87 is conserved. We describe the astrometry results in Section 4.3.

2.2. VERA GENJI sessions at 22 GHz (Mode-B)

In addition, VERA frequently observed M 87 at 22.2 GHz in the framework of the *GENJI* (*Gamma-Ray Emitting Notable AGN Monitoring by Japanese VLBI*) program (Nagai et al. 2013). This is a dense monitoring program of several bright γ-ray AGN jets including M 87 with VERA starting from October 2010, which takes advantage of the usual calibrator time for VERA's Galactic maser astrometry observations. Between September 2011 and September 2012, M 87 was routinely monitored with the *GENJI* mode typically every 2–3 weeks (hereafter we term these sessions as *Mode-B*). Some of the data were not useful because of the lack of one or two stations, or due to only one or two scans available, preventing us from making reliable images and flux density measurements. Then, we selected the data in which all four of the VERA stations participated and

at least three or four scans are available at different hour angles. Through these selection criteria, we eventually obtained the *Mode-B* data at 18 epochs in total during this period. Total on-source time for this mode is typically ∼30 minutes with an allocated bandwidth of 16 MHz. For more detailed descriptions about the data analysis of the *GENJI* data, see Nagai et al. (2013).

For all of the *Mode-A* and *Mode-B* data sets, images were created in DIFMAP software with iterative CLEAN and phase/amplitude self-calibration. The resultant amplitude corrections remained stable within ∼10% over time at each station, the level of which is consistent with a typical accuracy of the system temperature measurements for VERA. We thus adopt 10% error for the amplitude uncertainty for the VERA data. The resultant synthesized beams with the naturally-weighted scheme were typically 1.3×0.8 mas in a position angle (P.A.)$= -40^\circ$ and 0.65×0.40 mas in P.A.$= -40^\circ$ at 22 and 43 GHz, respectively. Comparing image qualities at 22 GHz, image rms levels achieved by *Mode-A* are twice (or more) as good as those obtained by *Mode-B* mainly because of the longer integration time and better *uv*-coverage. We summarize the information about the VERA data in Table 1.

2.3. EVN data at 5 GHz

We observed M 87 with EVN at 9 epochs between March 2011 and October 2012 as a continuation of our M 87/HST-1 monitoring project starting from mid 2009 (Giovannini et al. 2011; Giroletti et al. 2012). The observation at each epoch typically lasted 4–8 hours, and the longest baselines were achieved from European stations to Shanghai, Arecibo and/or Hartebeesthoek. Overall, the data quality is adequate to warrant good signal-to-noise detections of the source structure. For all observations, the sky frequency was centered at 5.013 GHz and divided into eight sub-bands separated by 16 MHz each for an aggregate bit rate of 1024 Mbps. The data were correlated in real time at the Joint Institute for VLBI in Europe (JIVE) and automated data flagging and initial amplitude/phase calibration were also carried out at JIVE using dedicated pipeline scripts. The data were finally averaged in frequency within each IF, but individual IFs were kept separate to minimize bandwidth smearing. Similarly, the data were time-averaged to only 8 seconds to minimize time smearing. We produced final images in DIFMAP after several cycles of phase and amplitude self-calibration. Various weighting schemes were applied to the data to improve resolution in the core region and enhance the fainter emission in the HST-1 region. For the core region, uniform weights or natural weights were used without *uv*-tapering, which achieve angular resolutions typically between 1–3 mas. For the HST-1 region, we used natural weights with a Gaussian *uv*-tapering (typically a factor of 0.3 at a radius of 50 Mλ, which results in a beam size between 5–10 mas. Image rms noise levels estimated in a region far from the core are typically 0.1 mJy/beam or less with the natural weights. Regarding uncertainties on flux density measurements, we adopted 10% error for core flux density based on a typical EVN amplitude calibration accuracy. For HST-1, we conservatively assumed 30% uncertainty because analyses of the HST-1 region could contain a larger amount of deconvolution error due to its weak and extended nature. Details of the EVN

Table 1: VERA and EVN observations of M 87

Array	Date	Date (MJD)	Beam (mas×mas, deg) (a)	rms $\left(\frac{\mathrm{mJy}}{\mathrm{beam}}\right)$ (b)	Mode (c)
43GHz	2012 Feb 24	55981	$0.65 \times 0.41, -41$	1.9	A
VERA	2012 Mar 16	56002	$0.63 \times 0.40, -40$	2.8	A
	2012 Mar 21	56007	$0.68 \times 0.44, -39$	1.2	A
	2012 Apr 05	56022	$0.65 \times 0.43, -43$	1.9	A
	2012 Apr 27	56044	$0.68 \times 0.44, -46$	1.8	A
	2012 May 17	56064	$0.65 \times 0.45, -45$	1.3	A
22GHz	2011 Sep 03	55808	$1.32 \times 0.80, -32$	5.5	B
VERA	2011 Sep 07	55811	$1.41 \times 0.77, -35$	2.9	B
	2011 Sep 09	55813	$1.34 \times 0.77, -35$	4.1	B
	2011 Oct 15	55849	$1.41 \times 0.80, -35$	2.7	B
	2011 Nov 05	55870	$1.31 \times 0.76, -37$	4.2	B
	2011 Dec 04	55899	$1.39 \times 0.84, -38$	2.3	B
	2011 Dec 20	55915	$1.41 \times 0.90, -18$	2.9	B
	2012 Jan 23	55949	$1.29 \times 0.87, -43$	1.6	B
	2012 Feb 24	55981	$1.40 \times 0.76, -40$	1.1	A
	2012 Feb 27	55984	$1.27 \times 0.89, -50$	1.8	B
	2012 Feb 28	55985	$1.57 \times 0.70, -43$	5.2	B
	2012 Mar 16	56002	$1.33 \times 0.84, -45$	2.7	A
	2012 Mar 21	56007	$1.40 \times 0.82, -36$	1.1	A
	2012 Apr 01	56018	$1.25 \times 0.96, -35$	2.0	B
	2012 Apr 05	56022	$1.39 \times 0.82, -40$	1.6	A
	2012 Apr 19	56036	$1.24 \times 0.85, -44$	2.7	B
	2012 Apr 23	56040	$1.50 \times 0.82, -25$	4.4	B
	2012 Apr 27	56044	$1.44 \times 0.84, -40$	1.5	A
	2012 May 17	56064	$1.36 \times 0.84, -40$	1.7	A
	2012 May 23	56070	$1.43 \times 0.78, -44$	2.6	B
	2012 Jun 21	56099	$1.29 \times 0.83, -53$	8.1	B
	2012 Aug 29	56168	$1.32 \times 0.96, -58$	8.2	B
	2012 Sep 13	56183	$1.34 \times 1.04, -55$	5.2	B
	2012 Sep 23	56193	$1.41 \times 0.78, -32$	3.9	B
5GHz	2011 Mar 09	55629	$3.05 \times 2.10, -67$	0.044	–
EVN	2011 Apr 12	55663	$2.71 \times 1.53, 86$	0.092	–
	2011 Jun 02	55714	$1.42 \times 1.05, -11$	0.135	–
	2011 Aug 25	55798	$3.09 \times 1.29, -73$	0.133	–
	2011 Oct 17	55851	$6.21 \times 2.29, -48$	0.099	–
	2012 Jan 10	55936	$1.63 \times 1.16, -72$	0.070	–
	2012 Mar 20	56006	$1.83 \times 1.67, 66$	0.054	–
	2012 Jun 19	56097	$2.82 \times 1.37, -89$	0.094	–
	2012 Oct 09	56209	$3.27 \times 2.29, -85$	0.078	–

Notes. Columns: (a) size of a synthesized beam with a naturally-weighted scheme; (b) rms image noise level at a region far from the core with the beam (a); (c) VERA observation mode for each epoch. "A" represents the dedicated mode, while "B" indicates the GENJI mode.

data are also summarized in Table 1.

2.4. SMA data at 230 GHz

The 230 GHz (1.3 mm) light curve was obtained at the SMA near the summit of Mauna Kea (Hawaii). M 87 is included in an ongoing monitoring program at the SMA to determine the flux densities of compact extragalactic radio sources that can be used as calibrators at mm wavelengths (Gurwell et al. 2007). Observations of available potential calibrators are observed for 3 to 5 minutes, and the measured source signal strength calibrated against known standards, typically solar system objects (Titan, Uranus, Neptune, or Callisto). Data from this program are updated regularly and are available at the SMA website[3]. Most of the SMA measurements were obtained in its compact array configuration and the typical angular resolution is about ∼3 arcseconds.

3. Fermi-LAT Data: Selection and Analysis

The *Fermi*-LAT is a pair-conversion telescope operating from 20 MeV to > 300 GeV. Further details about the *Fermi*-LAT are given in Atwood et al. (2009). The LAT data reported in this paper were collected from 2011 February 1 (MJD 55593) to 2012 September 30 (MJD 56200). During this time, the *Fermi* observatory operated almost entirely in survey mode. The analysis was performed with the `ScienceTools` software package version v9r32p5[4]. The LAT data were extracted within a 10° region of interest centred at the radio location of M 87. Only events belonging to the 'Source' class were used. The time intervals when the rocking angle of the LAT was greater than 52° were rejected. In addition, a cut on the zenith angle ($< 100°$) was applied to reduce contamination from the Earth limb γ rays, which are produced by cosmic rays interacting with the upper atmosphere. The spectral analysis was performed with the instrument response functions `P7REP_SOURCE_V15`[5] using an unbinned maximum-likelihood method implemented in the Science tool `gtlike`. A Galactic diffuse emission model and isotropic component, which is the sum of an extragalactic and residual cosmic ray background, were used to model the background[6]. The normalizations of both components in the background model were allowed to vary freely during the spectral fitting.

We evaluated the significance of the γ-ray signal from the sources by means of the maximum-

[3]http://sma1.sma.hawaii.edu/callist/callist.html

[4]http://fermi.gsfc.nasa.gov/ssc/data/analysis/documentation/

[5]http://www.slac.stanford.edu/exp/glast/canda/lat_Peformance.htm

[6]http://fermi.gsfc.nasa.gov/ssc/data/access/lat/BackgroundModels.html

likelihood test statistic TS = 2Δlog(likelihood) between models with and without a point source at the position of M 87 (Mattox et al. 1996). The source model used in `gtlike` includes all of the point sources from the second *Fermi*-LAT catalog (2FGL; Nolan et al. 2012) that fall within 15° of the source. The spectra of these sources were parametrized by power-law functions, except for 2FGL J1224.9+2122 (4C 21.35) and 2FGL J1229.1+0202 (3C 273), for which we used a log-parabola as in the 2FGL catalogue. A first maximum-likelihood analysis was performed to remove from the model the sources having TS < 25 and/or the predicted number of counts based on the fitted model $N_{pred} < 3$. A second maximum-likelihood analysis was performed on the updated source model. In the fitting procedure, the normalization factors and the photon indices of the sources lying within 10° of M 87 were left as free parameters. For the sources located between 10° and 15°, we kept the normalization and the photon index fixed to the values from the 2FGL catalogue.

Integrating over the period from 2011 February 1 to 2012 September 30 (MJD 55593–56200), the fit with a power-law model in the 0.1–100 GeV energy range results in a TS = 134, with an integrated average flux of $(2.22 \pm 0.43) \times 10^{-8}$ ph cm^{-2} s^{-1} and a photon index of $\Gamma = 2.25 \pm 0.10$. Taking into account the detection significance over the whole analysed period, we produced the γ-ray light curves with 1-month and 2-month time bins. This choice of binning is compatible with those adopted in the previous M 87 studies with LAT data (Abdo et al. 2009; Abramowski et al. 2012), and also reasonable for a comparison with the observed month-scale VHE activity in 2012. For each time bin, the spectral parameters for M 87 and for all the sources within 10° from it were frozen to the value resulting from the likelihood analysis over the entire period. In the light curve with the 2-month time bins, if TS < 10, 2σ upper limits were evaluated, while only bins with TS > 10 are selected in the light curve with the 1-month time bins. We describe the results of the LAT light curves in Section 4.2.

Dividing the 1-month bins with higher flux in 5-day sub-bins, the highest flux of $(10.4 \pm 4.8) \times 10^{-8}$ and $(8.6 \pm 3.4) \times 10^{-8}$ ph cm^{-2} s^{-1} was detected on 2011 October 12-16 and 2012 January 16-20, respectively (these sub-bin data also show TS>10). By means of the `gtsrcprob` tool, we estimated that the highest energy photon emitted from M 87 (with probability > 90% of being associated with the source) was observed by LAT on 2011 April 7, at a distance of 0.09° from the source and with an energy of 254.0 GeV, extending into the VHE range.

4. Results

4.1. Milliarcsecond scale images

Figure 1 shows VLBI images for M 87 during the elevated VHE state in March 2012. The large scale jet structure down to HST-1 was clearly detected with EVN, while VERA resolved the innermost region.

The obtained EVN jet images within several hundreds of mas from the nucleus are in good

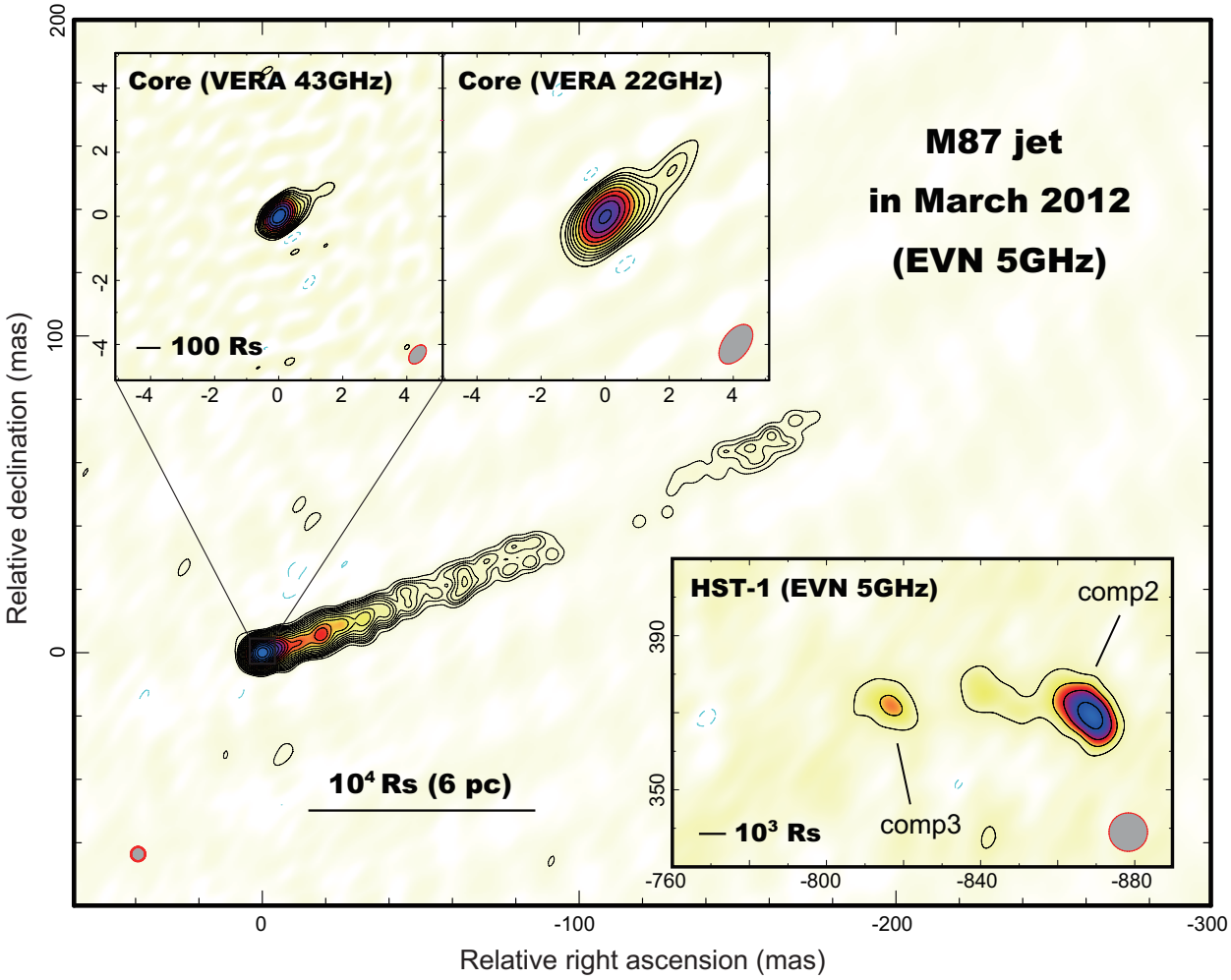

Fig. 1.— Montage of VLBI images of the M 87 jet during the elevated VHE γ-ray state in 2012 March. The main (global) image was obtained with EVN at 5 GHz (on March 20). The bottom right inset indicates a close-up view toward the HST-1 region. The nomenclatures of the two main features (comp2 and comp3) are based on Giroletti et al. (2012). The upper left two insets indicate VERA images for the core at 22 and 43 GHz (on March 21). For the EVN images, a circular Gaussian beam of 4.5 mas is used for the global structure (bottom left in the image), while a 10.0 mas circular beam is applied for HST-1 (bottom right in the HST-1 image). For the VERA images, the beam sizes are and 1.40×0.82 mas in P.A. $-36°$ and 0.68×0.44 mas in P.A. $-39°$ at 22 and 43 GHz, respectively (bottom right in each VERA image). For each image, contours start from -1, 1, 2, $2^{3/2}$, 4, $2^{5/2}$... times 3σ image rms levels (where 1σ are set to be 1.1 mJy beam^{-1} (22-GHz image), 1.2 mJy beam^{-1} (43-GHz image), 0.48 mJy beam^{-1} (EVN inner jet image) and 0.08 mJy beam^{-1} (EVN HST-1 image)) and increase by factors of $2^{1/2}$.

agreement with the well-known characteristics for this source; the jet is described by the bright radio core at the base with the edge-brightened collimated region (Junor et al. 1999; Ly et al. 2004; Dodson et al. 2006; Ly et al. 2007; Asada & Nakamura 2012; Hada et al. 2013). On the other hand, the VERA array is less sensitive to the extended emission (i.e., mostly resolved out) due to the lack of short baselines (> 60 Mλ and > 120 Mλ at 22 and 43 GHz respectively), so the detectable emission is generally concentrated within the central region (i.e., a few mas). Nevertheless, some of brighter features downstream of the core were indeed consistently detected at many of the analyzed epochs. Our preliminary kinematic measurements of these features with VERA suggest an apparent motion around $\sim 0.4\,c$ relative to the radio core (Hada 2013), which is similar to the value obtained in a previous VLBA study (Ly et al. 2007). However, these features have already existed from mid 2011 and we did not find any notable correlations with the 2012 VHE activity. Thus, here we do not describe further details on these features and the more dedicated treatment will be reported in a forthcoming paper.

In terms of the HST-1 region, we detected the detailed substructure in all of the analyzed EVN data, the characteristics of which are overall consistent with our previous study (Giroletti et al. 2012). We confirmed that the main emission features of HST-1 are still moving constantly at a superluminal speed of $\sim 4c$. While in Giroletti et al. (2012) we identified three main features (termed as comp1, comp2 and comp3 from the downstream side), in Figure 1 we can only see two main components. These features correspond to comp2 (the downstream, brighter one) and comp3 (the upstream, weaker one), respectively. The comp1, which was identified as the outermost feature in Giroletti et al. (2012), faded gradually and became below the noise limit at the beginning of 2012. While the emergence of new components from the upstream edge of HST-1 (around $(\mathrm{RA}, \mathrm{Dec}) = (-780, 350)$ mas from the core) were seen during the VHE events in 2005 and 2010, we did not find such a structural variation during the 2012 event.

4.2. MWL Light Curves

In Figure 2, we show a combined set of light curves of M 87 from radio to MeV/GeV γ-ray between MJD 55400 and MJD 56280. The vertical shaded area over the plots indicates a period between February 2012 and March 2012, where an elevated VHE state is reported by VERITAS (Beilicke et al. 2012). For the LAT data, we show the light curves produced with 1-month and 2-month time bins (including 2σ upper limits for the 2-month time bins). For the SMA data, we plot a light curve of the total flux densities. For the EVN 5-GHz data, we show the light curves for both the HST-1 region (integrated flux densities) and the core (peak flux densities when convolved by a 1.5-mas circular beam). In terms of the VERA data at 22/43 GHz, the light curves obtained by the *Mode-A/B* are combined into a single sequence. At each frequency, we provide both the integrated flux density and the peak flux density when convolved with a 0.6-mas circular Gaussian beam. Additionally, we plot an evolution of the spectral index for the peak flux density between 22 and 43 GHz.

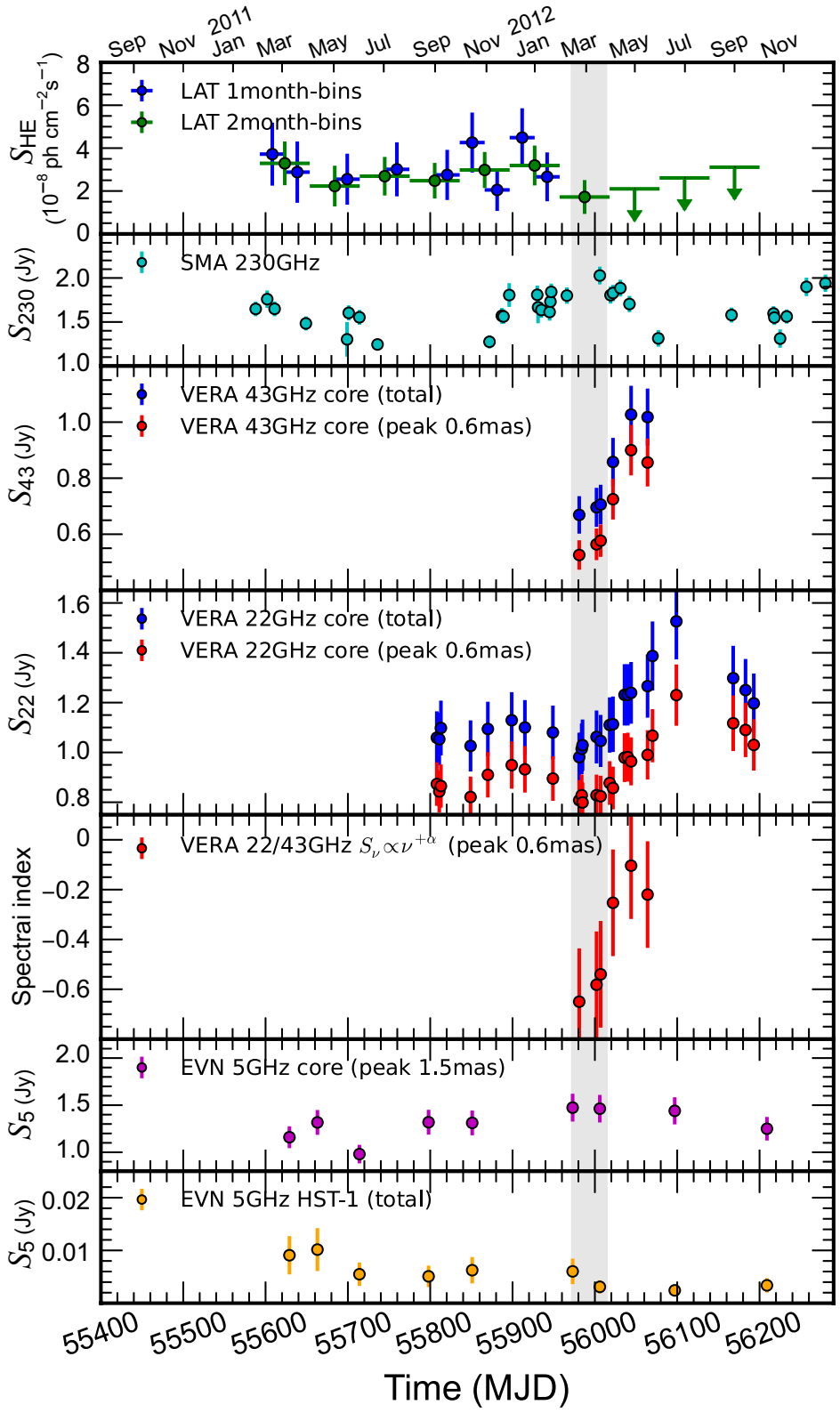

Fig. 2.— Multi-wavelength light curves of M 87 between February 2011 and December 2012. The vertical shaded area over the plots indicates a period of elevated VHE emission reported by Beilicke et al. (2012). See the text for more detailed description for the each panel of the light curve.

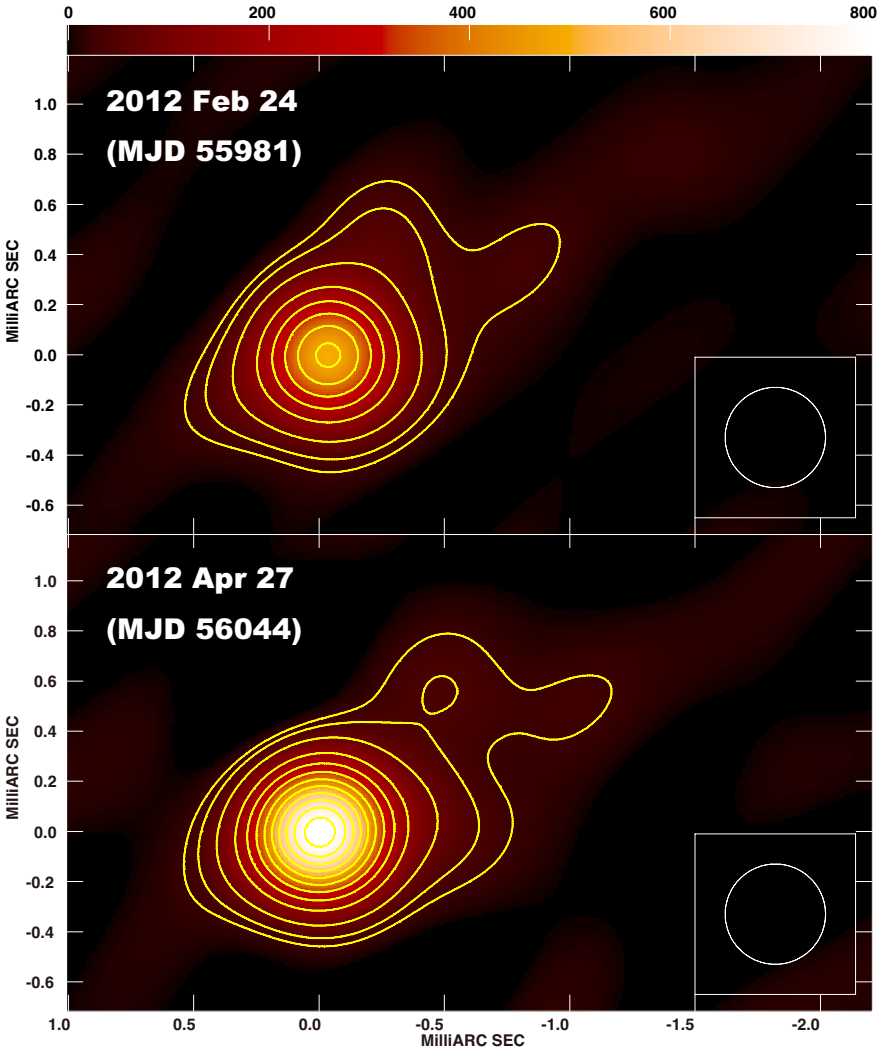

Fig. 3.— VERA 43-GHz images of the M 87 jet during the elevated VHE state in 2012. The images are convolved with a 0.4 mas diameter circular Gaussian beam (shown at the bottom-right corner of each image), the size of which is close to the FWHM of the minor axis of the synthesized beam. The range of intensities is represented both in color and with contours at levels of 800 mJy beam$^{-1}\times$ (0.01, 0.05, 0.1, 0.2, 0.3, 0.4, 0.5, 0.6, 0.7, 0.8, 0.9, 1.0).

Table 2: Flux density measurements with VERA at 22 and 43 GHz

Date	Date (MJD)	$S_{22,\mathrm{tot}}$ (mJy) (a)	$S_{22,\mathrm{peak}}$ $\left(\frac{\mathrm{mJy}}{\mathrm{beam}}\right)$ (b)	$S_{43,\mathrm{tot}}$ (mJy) (c)	$S_{43,\mathrm{peak}}$ $\left(\frac{\mathrm{mJy}}{\mathrm{beam}}\right)$ (d)	$\alpha_{22-43,\mathrm{peak}}$ (e)
2011 Sep 03	55808	1059 ± 106	873 ± 87			
2011 Sep 07	55811	1053 ± 105	843 ± 84			
2011 Sep 09	55813	1098 ± 110	865 ± 87			
2011 Oct 15	55849	1026 ± 103	821 ± 82			
2011 Nov 05	55870	1094 ± 109	910 ± 91			
2011 Dec 04	55899	1129 ± 113	949 ± 95			
2011 Dec 20	55915	1100 ± 110	932 ± 93			
2012 Jan 23	55949	1080 ± 108	895 ± 90			
2012 Feb 24	55981	981 ± 98	808 ± 81	669 ± 67	526 ± 53	-0.65 ± 0.21
2012 Feb 27	55984	1014 ± 101	828 ± 83			
2012 Feb 28	55985	1029 ± 110	799 ± 80			
2012 Mar 16	56002	1062 ± 106	828 ± 83	696 ± 70	564 ± 56	-0.58 ± 0.21
2012 Mar 21	56007	1046 ± 105	824 ± 82	706 ± 71	577 ± 58	-0.54 ± 0.21
2012 Apr 01	56018	1110 ± 111	877 ± 88			
2012 Apr 05	56022	1113 ± 111	857 ± 86	858 ± 86	725 ± 73	-0.25 ± 0.21
2012 Apr 19	56036	1231 ± 123	979 ± 98			
2012 Apr 23	56040	1204 ± 120	981 ± 98			
2012 Apr 27	56044	1239 ± 124	964 ± 96	1027 ± 103	900 ± 90	-0.10 ± 0.21
2012 May 17	56064	1266 ± 127	990 ± 99	1018 ± 102	856 ± 86	-0.22 ± 0.21
2012 May 23	56070	1387 ± 139	1067 ± 107			
2012 Jun 21	56099	1526 ± 153	1230 ± 123			
2012 Aug 29	56168	1298 ± 130	1117 ± 112			
2012 Sep 13	56183	1263 ± 126	1090 ± 109			
2012 Sep 23	56193	1197 ± 120	1072 ± 107			

Notes: (a) and (c) Integrated flux density of VERA images at 22 GHz and 43 GHz, respectively: (b) and (d) Peak flux density of VERA at 22 GHz and 43 GHz (with a 0.6-mas-diameter circular Gaussian convolving beam), respectively: (e) Spectral index calculated by $\log(S_{22,\mathrm{peak}}/S_{43,\mathrm{peak}})/\log(22.291/43.125)$.

Table 3: Flux density measurements with EVN at 5 GHz

Date	Date (MJD)	$S_{5,\mathrm{core}}$ $\left(\frac{\mathrm{mJy}}{\mathrm{beam}}\right)$ (a)	$S_{5,\mathrm{HST-1}}$ (mJy) (b)
2011 Mar 09	55629	1160 ± 116	9.1 ± 2.7
2011 Apr 12	55663	1317 ± 132	10.2 ± 3.6
2011 Jun 02	55714	981 ± 98	5.5 ± 1.7
2011 Aug 25	55798	1319 ± 132	5.1 ± 1.5
2011 Oct 17	55851	1312 ± 131	6.3 ± 1.9
2012 Jan 10	55936	1474 ± 147	6.0 ± 1.8
2012 Mar 20	56006	1463 ± 146	3.1 ± 0.9
2012 Jun 19	56097	1440 ± 144	2.4 ± 0.7
2012 Oct 09	56209	1250 ± 125	3.4 ± 1.0

Notes: (a) peak flux density of the core when convolved by a 1.5-mas-diameter circular Gaussian beam: (b) integrated flux density of the HST-1 region.

Thanks to the dense, complementary coverages of VERA and EVN, we revealed the detailed evolutions of the radio light curves for both the core and HST-1. The most remarkable finding in these plots is a strong enhancement of the radio core flux density at VERA 22 and 43 GHz that starts from MJD 55981 (2012 February 24). While the timing of the radio peak is delayed, the onset of the radio flare occurs coincidentally with the enhanced VHE activity. At 22 GHz, we further detected a subsequent decay stage of the brightness at the last three epochs. Also at 43 GHz, we detected possible saturation of the flux increase near the last epoch. Meanwhile, the EVN monitoring confirmed a constant decrease of the HST-1 luminosity. We also checked the light curve for the peak flux density of HST-1 (with a 10-mas-diameter convolving beam), but the overall trend is the same as that of the integrated flux density. We summarize the values of the measured flux with VERA and EVN in Table 2 and Table 3.

To better describe the structure of the core region, we created VERA 43-GHz images convolved with a circular Gaussian beam of 0.4-mas diameter (Figure 3), which are $\sim$30% super-resolution along the major axis of the synthesized beam. These images clearly indicate that the flux enhancement occurs within the central spatial resolution of 0.4 mas, corresponding to a linear scale of 0.03 pc or 56 R_{s}. During the period of the elevated VHE state, the SMA data at 230 GHz also appear to show a local maximum in its light curve, although we note that its angular resolution is significantly large (generally $\sim$1–3 arcseconds, containing both the core and HST-1).

Another notable finding by our monitoring is a frequency-dependent evolution of the radio core flare. Figure 4 summarizes a set of the radio light curves that are normalized by the "baseline level" of the radio flare at each frequency (i.e., the flux values on MJD 55981 at 22/43 GHz and on MJD 55936 at 5 GHz, after which the radio core starts to flare). This figure clearly indicates that

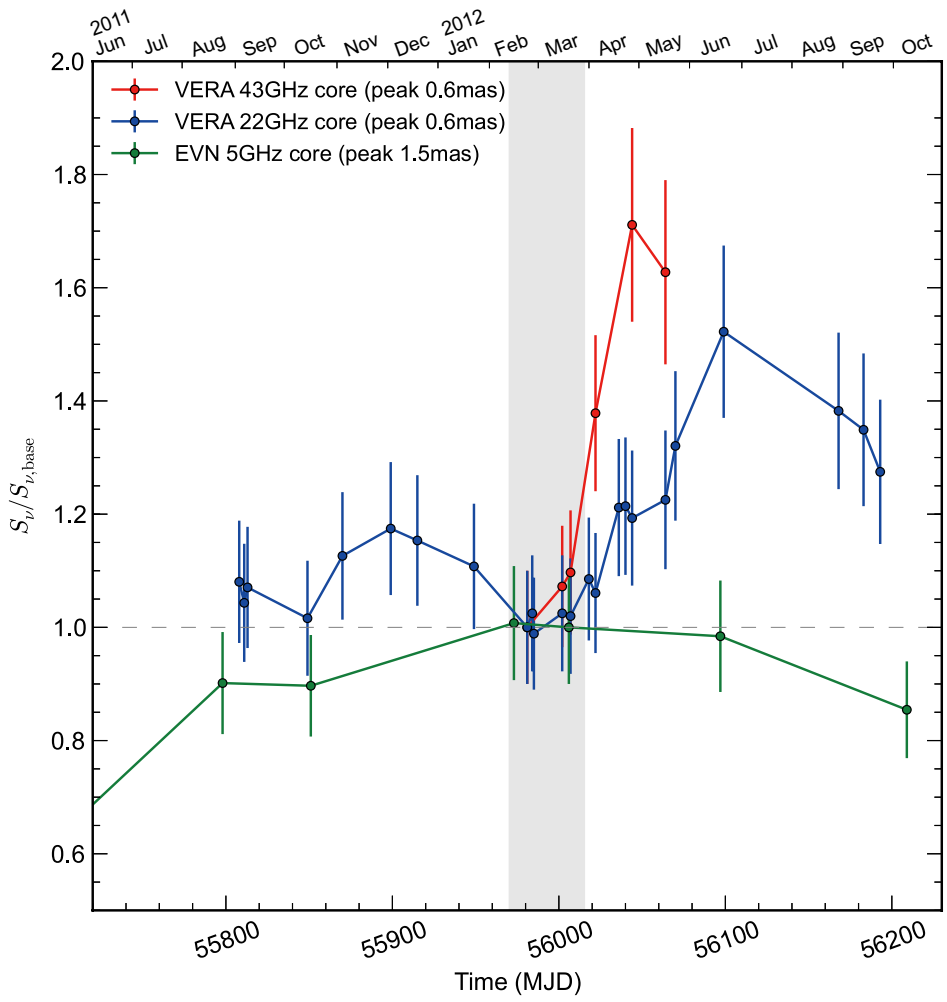

Fig. 4.— Normalized radio light curves of the M 87 core at 43 (peak 0.6 mas), 22 (peak 0.6 mas) and 5 GHz (peak 1.5 mas). The light curves at 43, 22 and 5 GHz are normalized to the flux values on MJD 55981, MJD 55981 and MJD 55936, respectively. The vertical shaded area over the plots indicates a period of the elevated VHE state reported by Beilicke et al. (2012)

the radio core brightens more rapidly with a larger amplitude as frequency increases. At 43 GHz, the flux density increased up to ∼70% for the subsequent two months (between MJD 55981 and MJD 56044) at an averaged rate of ∼35%/month, and afterward the growth seems to be saturated. On the other hand, the core flux density at 22-GHz progressively increased up to ∼50% (at least) for the subsequent four months (from MJD 55981 to MJD 56099) at a slower rate of ∼12%/month. Eventually, the spectral index of the radio core between the two frequencies changed continuously during the flaring event (from $\alpha \sim -0.6$ to ~ -0.1 for the peak flux with a 0.6-mas beam; see Figure 2). At 5 GHz, by contrast, the core remained virtually stable within the adopted error of 10%. This is the first time that such a frequency-dependent nature of the radio flare is clearly detected in the M 87 jet.

With regard to the MeV/GeV regime, the LAT light curves were stable up to February 2012 (both 1- and 2-month time bins), and we did not find any significant flux enhancement during the period of the VHE activity. The observed HE flux level was consistent with that seen in the earlier epochs (Abdo et al. 2009; Abramowski et al. 2012) within the adopted uncertainty. After March 2012, however, no significant emission was detected for the subsequent 6 months in the 1- and 2-month binned data, suggesting a change in the HE state after the VHE event. To quantify this, we analyzed the LAT data in two 6-month intervals, 2011 October-2012 March and 2012 April-September, following the same procedure described in Section 3. The fits resulted in 0.1-100 GeV fluxes of $(2.6 \pm 0.5) \times 10^{-8}$ ph cm^{-2} s^{-1} (TS = 56) and $(1.1 \pm 0.5) \times 10^{-8}$ ph cm^{-2} s^{-1} (TS = 10), respectively. This indicates a decrease in the HE flux by a factor of ~ 2 after the VHE event, in agreement with the level of decrease observed at VHE in 2012 April-May (Beilicke et al. 2012).

4.3. Astrometry of the core

Since the VERA *Mode-A* performed astrometry observations at both 22 and 43 GHz, these data enable us to examine the core shift effect during the VHE activity in 2012. The core-shift effect is expected as a natural consequence of the nuclear opacity effect if the radio core at each frequency corresponds to a surface of synchrotron-self-absorption (SSA) $\tau_{\rm ssa}(\nu) \sim 1$ (Königl 1981; Lobanov 1998; Hada et al. 2011).

In Figure 5, we show the result of our VERA astrometry for the M 87 radio core at 22 and 43 GHz, which are measured relative to the radio core of M 84 at each frequency. For each data, we defined the core position as follows. For M 87, we convolved the self-calibrated images by a 0.6-mas/0.4-mas-circular Gaussian beam at 22/43 GHz, the length of which is virtually equal to that of the minor axis of synthesized beam at each frequency. Then, we determined a brightness centroid of the image by fitting a Gaussian model with the AIPS task JMFIT. For M 84, we used its phase-referenced images instead of self-calibrated ones. Regarding position errors adopted for each data point in Figure 5, here we considered a root-sum-square of individual errors from the peak-to-noise ratio of the M 84 phase-referenced image, tropospheric residuals, ionospheric residuals and geometrical errors.

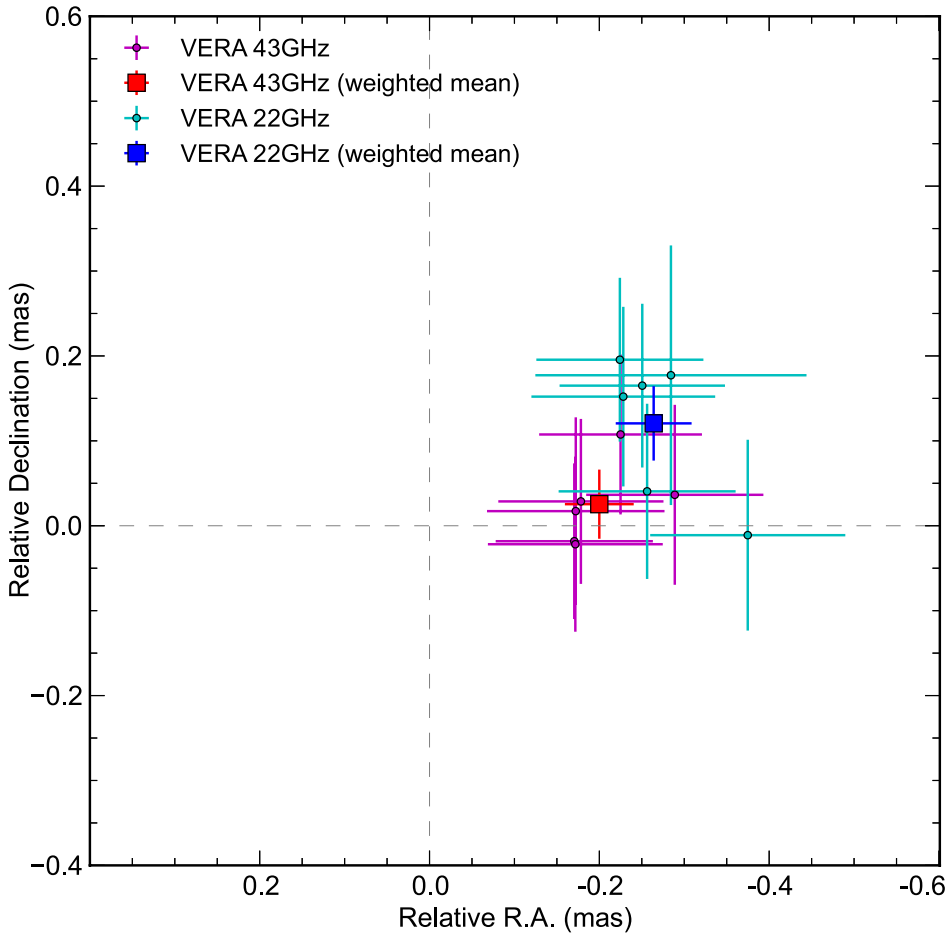

Fig. 5.— VERA astrometry of the M 87 core position at 22 and 43 GHz with respect to the core position of M 84. A set of the cyan circles with the error bars indicates the observed core positions at 22 GHz, while the other data set with the magenta circles represents the core positions at 43 GHz. We show all of the six epochs (2012 February 24, March 16, 21, April 5, 27 and May 17) obtained by the *Mode-A* at each frequency. The error budget for each data point includes the following terms; the peak-to-noise ratio of the phase-referenced image of M 84, tropospheric residual, ionospheric residual and geometrical errors. We also plot a weighted mean position of the core over the six epochs as blue/red rectangles at 22/43 GHz, respectively. As the coordinate origin of this plot, the nominal phase-tracking center for M 87 $\alpha_{\rm J2000} = 12^{\rm h}30^{\rm m}49\overset{\rm s}{.}4233830$ and $\delta_{\rm J2000} = 12^{\circ}23'28\overset{''}{.}043840$ is used.

Although the position uncertainty estimated for each data point is not sufficiently small (a level of 0.1–0.15 mas), our multi-epoch, collective data set reveals a noticeable trend that the 22-GHz core of M 87 tends to be located northeast of the 43-GHz core. At each frequency, we derived a weighted-mean position of the M 87 core over the analyzed epochs to be $(x_{43}, y_{43}) = (-199 \pm 41, 25 \pm 41)$ μas (a red square in Figure 5) and $(x_{22}, y_{22}) = (-263 \pm 44, 120 \pm 45)$ μas (a blue square in Figure 5) relative to the nominal phase-tracking center of M 87. These values yield a time-averaged separation of the core between 22 and 43 GHz to be $(\Delta x_{22-43},\ \Delta y_{22-43}) = (64, 95)$ μas, corresponding to a projected distance of (0.005, 0.008) pc or (9, 13) $R_{\rm s}$. This results in a position angle of the core shift to be 326°, which is well within a wide opening angle (between P.A.$\sim$255° and $\sim$340°) observed at the M 87 jet base with higher-angular-resolution studies (Junor et al. 1999; Hada et al. 2013).

To be accurate, however, we should be cautious about the following additional position uncertainties. As described in Hada et al. (2011), the structure of the reference source M 84 is elongated in the north-south direction. This may produce a core shift of M 84 itself in declination (although its amount should be less than 10 μas between 22 and 43 GHz; see Hada et al. 2011). Also, it is empirically suggested that astrometric measurements with VERA tend to leave slightly larger position errors in declination than in right ascension due to the residuals of zenith tropospheric delay estimations (e.g., Honma et al. 2007; Hirota et al. 2007). Thus, the actual position uncertainties of the M 87 core in declination could be somewhat larger than those adopted in Figure 5.

Another concern is that the amount of the core shift obtained with VERA (Δx_{22-43}, Δy_{22-43}) could be slightly larger than that of the true core shift, since the "radio core" defined by VERA, a beam size of which is typically $\sim$2–3 times larger than that of VLBA, would contain more amounts of the optically thin jet emission beyond the $\tau_{\rm ssa}(\nu) \sim 1$ surface. Such a blending of the optically thin jet should be more significant at 22 GHz as hinted by the result that the core spectra obtained by VERA tend to be steeper than those of VLBA. Then, in order to estimate a potential (artificial) increase of the core position shift due to the blending of the optically-thin jet, we performed the following test; at 22 GHz, we convolved the M 87 structure by many different beam sizes with diameters ranging from 0.6 to 2.4 mas in incremental steps of 0.2 mas. Then, we plotted systematic changes of brightness-peak position (i.e., effective core position at each resolution) as a function of beam size. Using this plot, we found a progressive position shift of the brightness peak (toward the downstream side) to be $(\sim 6, \sim 3)$ μas per 0.2 mas (in (x, y) directions) for a range of beam size from 0.6 to 2.4 mas. This implies that a core shift of $(\sim 6, \sim 3) \times \frac{0.6 \text{ mas}}{0.2 \text{ mas}} = (\sim 18, \sim 9)$ μas can be artificially caused by the blending effect of the unresolved optically thin jet within a beam size of 0.6 mas.

Therefore, we conclude that the true core shift of M 87 should be a level of 40–50 μas in the right ascension, while in declination 80–90 μas is estimated with a slightly larger uncertainty. In terms of the component in right ascension, a quite similar level of core shift is obtained in the previous measurements with VLBA ($\sim$30 μas between 22 and 43 GHz; Hada et al. 2011).

In principle, our multi-epoch astrometry allows us to investigate a time evolution of the core

position, which is particularly interesting to explore during a radio flaring stage. However, the observed small position changes relative to the errors make a reliable examination difficult among individual epochs. Conservatively, in the this paper we can say that the core position is stable within a scale of 0.3 mas (corresponding to $\sim$40 $R_{\rm s}$ or $\sim$0.02 pc) during the radio flare by taking into account the maximum extent of the core position scatters in these data.

5. Discussion

5.1. The location of the 2012 VHE activity

The location and the origin of the γ-ray emission up to VHE from M 87 have been under active debate in recent years. In the 2005 episode, the VHE flare was accompanied by radio-to-X-ray flares from HST-1 (Harris et al. 2006) with the ejections of superluminal radio features (Cheung et al. 2007), leading to a scenario that the VHE emission originates in HST-1 (Stawarz et al. 2006; Cheung et al. 2007; Harris et al. 2008, 2009). In contrast, contemporaneous flux increases at VHE, from the X-ray core and from the 43-GHz core during the 2008 episode suggest that the VHE flare originates in the jet base (Acciari et al. 2009). A coincident enhancement of the X-ray core flux also occurred during the VHE flare in 2010 (Harris et al. 2011; Abramowski et al. 2012) together with a possible flux density increase from the radio core (Hada et al. 2012). These results also tend to favor the scenario that the VHE emission originates in the jet base. However, the detection of the new component emergence from HST-1 near the VHE event again evoked the possibility that the HST-1 region is related to the active event in 2010 (Giroletti et al. 2012).

During the period of the elevated VHE activity in 2012 (Beilicke et al. 2012), we detected a significant flux density increase from the radio core at both 43 and 22 GHz. Following the 2008 episode this is the second time where a VHE event accompanied a remarkable radio flare from the core. Meanwhile, the radio luminosity of the HST-1 region was continuously decreasing, and we did not find any hints of the emergence of new components from HST-1 as seen in 2005 and 2010. These results strongly suggest that the VHE activity in 2012 is associated with the core at the jet base, while HST-1 is an unlikely source. We should note that these remarkable flares are very rare also in radio bands (see the supporting material in Acciari et al. 2009), so it is unlikely that an observed joint radio/VHE correlation is a chance coincidence, while the low statistics of the LAT light curves still do not allow conclusive results on the HE-VHE connection. Moreover, we also emphasize the clear detection of a progressive change of the radio core spectral index after the VHE high state using three frequencies. This was not revealed in the previous radio flare during the 2008 VHE event, where there was only single radio coverage at 43 GHz.

Currently a variety of mechanisms have been proposed for the VHE γ-ray production from the jet base of M 87 based on both leptonic and hadronic origins. In what follows, we will briefly discuss the compatibility of these models with the VHE activity in 2012, specifically from the point of view of high-resolution radio observations. On the basis of VLBI data, we can summarize

some of the key observational constraints as follows; first, the VERA 43-GHz images indicate the size of the radio flaring region to be smaller than the central spatial resolution of ∼0.4 mas (56 $R_{\rm s}$ or 0.03 pc), which is consistent with a source size implied by the observed month-scale VHE variability in 2012 ($R_{\rm var} \sim c\delta t_{\rm var} \sim 7.5 \times 10^{16}\delta$ cm or 42δ $R_{\rm s}$ for $t_{\rm var} \sim 30$ days, where δ is the Doppler factor); second, M 87 has a very short BH-to-core distance (∼a few tens of $R_{\rm s}$; Hada et al. 2011) and the jet launch/collimation region is beginning to be resolved at its base (Junor et al. 1999; Asada & Nakamura 2012; Hada et al. 2013); third, while the maximum of the radio flare is delayed, the onset of the radio brightening in 2012 occurs simultaneously with the VHE enhancement, indicating that the two emission regions are not spatially separated. Therefore, any compatible scenarios with the 2012 VHE activity should satisfy these conditions obtained by the radio observations.

Some of the existing models ascribe the VHE production to extremely compact regions (BH magnetosphere; Neronov & Aharonian (2007); Rieger & Aharonian (2008); Levinson & Rieger (2011): multi-blob in jet launch/formation region; Lenain et al. (2008): mini-jets in the main jet; Giannios et al. (2010): or red-giant-stars/jet-base interactions; (Barkov et al. 2010)). These models well explain the rapid (a few days) variability observed in the previous VHE flares in 2005, 2008 and 2010. Also, these models are able to avoid the internal γ (VHE) – γ (IR) absorption problem near the black hole since M 87 has only a weak IR nucleus (Neronov & Aharonian 2007; Brodatzki et al. 2011). However, as far as we consider the case in 2012, the size of the associated region expected from these models (typically of the order of $R_{\rm s}$ but as small as ∼0.01 $R_{\rm s}$ in Lenain et al. 2008) seems to be significantly smaller than that suggested by VLBI and the observed longer timescale of the VHE variability. Note that a contemporaneous mm-VLBI observation at 230 GHz during the 2012 event also suggests possible constraint on the associated size to be a similar spatial scale ($\gtrsim$0.3 mas; Akiyama et al. in prep.).

On a larger scale (but still unresolved with cm-VLBI), Georganopoulos et al. (2005) proposed a blazar-type, two-zone emission model where the VHE emission is produced in the upstream, faster jet while the lower-energy emission originates in the downstream, decelerating part of the jet. This model can reproduce the VHE data of M 87 if the jet decelerates its bulk Lorentz factor from $\Gamma_{\rm j} \sim 20$ to $\Gamma_{\rm j} \sim 5$ over a length of ∼0.1 pc at the jet base. However, the previous VLBA monitoring studies as well as our VERA monitor often show sub-relativistic motions and do not support such a very fast speed near the jet base (Reid et al. 1989; Dodson et al. 2006; Ly et al. 2007; Kovalev et al. 2007), although one cannot completely rule out faster motions in the jet base region that cannot be resolved with current cm-VLBI. The application of this model for the jet base of M 87 (i.e., jet launch region within $\lesssim 100$ $R_{\rm s}$ from the black hole) seems to be also incompatible with the current theoretical paradigm on the jet production, where the launched jet is expected to start acceleration on this scale (e.g., McKinney 2006; Komissarov et al. 2007).

Another blazar-type scenario in the sub-parsec jet is proposed by Tavecchio & Ghisellini (2008), where the radio-to-GeV emission of M 87 originates in the interior, spine part of the jet while the VHE emission is produced in the surrounding layer. However in their steady state model, whether

the model can explain the observed simultaneous radio/VHE correlation or not has not been well investigated yet because the emission regions associated with radio and VHE are spatially separated from each other.

Similarly, the existing hadronic-based VHE emission models (e.g., Reimer et al. 2004; Barkov et al. 2010; Reynoso et al. 2011) do not necessarily expect obvious radio/VHE correlations because the radio emission is usually ascribed to be the synchrotron emission from the electrons that are not responsible for the VHE production. To test the viability of these (both multi-zone and multi-particle) models, more detailed considerations including their time-dependent behaviors through radio to VHE γ-ray would be necessary.

Interestingly, Abdo et al. (2009) showed that a broadband SED of M 87 through radio to VHE (at a relatively moderate state) can be reasonably reproduced by a simple, homogeneous one-zone synchrotron self-Compton (SSC) jet model using a roughly comparable source size ($\lesssim$0.1 mas) to the one suggested in the 2012 case. In principle, one can also accept coincident radio/VHE correlations in this context. One-zone SSC models also explain the broadband SEDs in the other known γ-ray detected FR-I radio galaxies 3C 84/NGC 1275 (up to TeV; MAGIC Collaboration et al. 2013) and Centaurus A (up to GeV; Chiaberge et al. 2001; Abdo et al. 2010), implying these sources to be misaligned counterparts of BL Lac objects. However, such single-zone approaches to misaligned objects derive systematically smaller bulk Lorentz factors ($\Gamma_{\rm j} < 5$) than those generally required in BL Lacs ($\Gamma_{\rm j} > 10$), which may pose a conflict with the radio-loud AGN unification paradigm (Urry & Padovani 1995). This caveat, along with limb-brightened jet structures observed in some radio galaxies (e.g., Junor et al. 1999; Nagai et al. 2014), indeed led to the preferable use of more sophisticated models with multiple jet parts at different velocities (e.g., Georganopoulos et al. 2005; Tavecchio & Ghisellini 2008) or with multiple substructures (e.g., Lenain et al. 2008; Giannios et al. 2010). For M 87, such multi-zone models also should be viable, but more extended theoretical consideration would be needed (e.g., ways to produce the joint radio/VHE correlation).

5.2. The nature of the radio flare

Our multi-frequency radio monitoring revealed a frequency-dependent property of the radio light curves for the M 87 core; as frequency decreases, the luminosity slowly increases with a smaller amplitude enhancement, resulting in a larger time delay/lag until reaching its peak. While this type of behavior is often seen in blazars (e.g., Orienti et al. 2013), the present study is the first clear confirmation for the M 87 jet. Such a behavior is often explained by the creation of a plasma condensation (presumably induced by the VHE event at the jet base), which subsequently expands and propagates down the jet under the effect of SSA (Marscher & Gear 1985; Valtaoja et al. 1992). In this idea, the stronger SSA opacity at the jet base causes a delayed brightening of the radio flux density at lower frequencies. The light curve at each frequency reaches its maximum when the newborn component passes through the $\tau_{\rm ssa}(\nu) \sim 1$ surface (i.e., the radio core at the corresponding frequency). Afterward, the light curve enters a decay phase due to the adiabatic expansion loss

(plus additional cooling effects, if any). A self-absorbed synchrotron response of radio core light curve in M 87 is also suggested for the 2008 episode (Acciari et al. 2009), where the delayed increase of the 43-GHz core flux relative to the VHE peak was reasonably reproduced by a phenomenological modeling of a self-absorbed plasma at the jet base.

On the other hand, we did not see any flux enhancement from the 5 GHz core of M 87. This implies that the newborn component was short-lived and incorporated into the uniform (underlying) jet before reaching the $\tau_{\rm ssa}(5\ {\rm GHz}) \sim 1$ surface, resulting in the absence of any explicit emergences of knots or notable features from the core during this period. We note that the inner jet region of M 87 shows a relatively smooth brightness distribution, in agreement with low power (FR Is and BL Lacs) jet properties, while jets in high power sources (FR IIs and quasars) show clear evidence of complex substructures (Giovannini et al. 2001).

One of the important results of our observations is that we independently obtained both the core shift and the time-lag of the multi-frequency flare simultaneously. As examined by Kudryavtseva et al. (2011), the time-lag of the radio flare is directly related to the amount of core shift divided by the speed of the propagating shock or component. In turn, this means that we can now estimate the speed of the propagating component in the following way using the core shift and the time-lag;

$$\begin{aligned} \beta_{\rm app,43\to22} &= \frac{\Delta r_{\rm proj,43-22}}{c\Delta t_{43-22}} \\ &= 0.97 \left(\frac{\Delta\theta_{43-22}}{0.1\ {\rm mas}}\right) \left(\frac{\Delta t_{43-22}}{10\ {\rm days}}\right)^{-1} \left(\frac{D_{\rm source}}{16.7\ {\rm Mpc}}\right) \end{aligned}$$

where $\beta_{\rm app,43\to22}$, $\Delta r_{\rm proj,43-22}$, $\Delta\theta_{43-22}$, Δt_{43-22} and $D_{\rm source}$ represent a proper (projected) motion of the propagating component from the 43-GHz core to the 22-GHz one, a projected separation of 43/22 GHz cores (in physical unit/in angular unit), a time-lag of the light curve peaks between 43 and 22 GHz, and a source distance, respectively. For $\Delta\theta_{43-22}$, our VERA astrometry obtained a level of $\Delta\theta_{43-22}\sim$0.04–0.09 mas during the radio flare. Regarding Δt_{43-22}, although the obtained light curves are not adequate to specify the exact date of the peak at both 22 and 43 GHz, we can still reasonably constrain a likely range of the peak date to be between MJD 56044 and MJD 56064 at 43 GHz, and between MJD 56099 and MJD 56168 at 22 GHz, respectively. This results in the maximum allowed range of Δt_{43-22} to be 35 days $\lesssim \Delta t_{43-22} \lesssim$ 124 days. Therefore, we finally derive a likely range of $\beta_{\rm app,43\to22}$ to be $\sim$0.04c–0.22c. This indicates that the newborn component propagating through the cores between 43 and 22 GHz is not highly relativistic. Notably, many previous kinematic observations of M 87 obtained a similar speed ($\lesssim 0.05\ c$; Kovalev et al. 2007) or a slightly higher value ($0.25 - 0.4\ c$; Ly et al. 2007) in the jet a few mas (subparsec) downstream of the core. A value around $\sim$0.4 c (relative to the core) at a few mas beyond the core was also measured in our VERA data (Hada 2013), suggesting a possible acceleration process in the jet flow on this scale. On the other hand, the derived sub-luminal speed of the newborn component is significantly smaller than the super-luminal features appeared from the core during the previous VHE event in 2008 ($\sim$1.1c; Acciari et al. 2009), where the peak VHE flux is >5 times higher

than that in 2012. If we assume that propagating shocks or component motions traced by radio observations reflect the bulk velocity flow, this may suggest that the stronger VHE activity is associated with the (episodic) production of the higher Lorentz factor jet. We note that the M 87 jet is misaligned ($i \sim 15^\circ - 25^\circ$; Acciari et al. 2009), but such a positive correlation between the jet speed and the observed VHE flux is plausible because the jet emission is still "beamed" toward us ($\delta \sim$a few) for such mildly relativistic speeds ($\Gamma \lesssim 2$) in the suggested i range.

We note that the above discussion applies to a thin-shock case where the thickness (i.e., the size along the jet) of the propagating feature is smaller than the (de-projected) separation between the 43 and 22-GHz cores in order to allow a non-zero time delay (Δt_{43-22}) in their light curve peaks. Also, here we considered only a time-averaged value for the core shift for simplicity. However, the amount of core shift can be variable especially during the radio flaring event (Kovalev et al. 2008), because the creation of such features may locally change the particle number density, the magnetic field strength and thus the SSA optical depth at the jet base. The position accuracies in the present study are still not enough to explore the core-shift variations among the individual epochs, but this effect should be of interest to test with a more suitable astrometry technique (e.g., Korean VLBI Network (KVN); Lee et al. 2014: or KVN+VERA joint array; Sawada-Satoh 2013). This will enable us to bring further insights into the nature of the flaring core as well as the γ-ray production in the formation and collimation region of the M 87 jet.

6. Summary

We reported our intensive, high-resolution radio monitoring observations of the M 87 jet with VERA at 22/43 GHz and EVN at 5 GHz during the elevated VHE state in early 2012 jointly with the contemporaneous MeV/GeV light curves obtained by *Fermi*-LAT. We summarize our main results as follows;

1. We detected a strong increase of the radio flux density from the jet base (radio core) at both 22 and 43 GHz coincident with the elevated VHE activity. Meanwhile, we confirmed that the HST-1 region remained quiescent in terms of its flux density and mas-scale structure. These results strongly suggest that the VHE event in 2012 originates in the jet base within the central resolution element of 0.4 mas = 0.03 pc = 56 $R_{\rm s}$ near the supermassive black hole, while HST-1 is unlikely.

2. We discovered a clear frequency-dependent evolution of the radio core light curves at 43, 22 and 5 GHz. The radio flux increased more rapidly at 43 GHz with a stronger amplitude, while the observed light curve at 5 GHz remained stable. Taking advantage of the dual-beam astrometry technique with VERA, we also detected a core shift between 22 and 43 GHz. These results suggest that a new radio-emitting component was created near the black hole during the VHE event, and propagating through the opaque cores at these frequencies. Since we did not see any flux/structural variations for the 5-GHz core, this implies that the newborn

component was quenched before reaching the 5-GHz core. This confirms that jets in low power radio sources generally show a uniform brightness distribution because knotty features are short-lived and disappear very soon.

3. In terms of the MeV/GeV regime, the LAT light curves were stable during the analysed period before the VHE event, and we did not find any significant flux enhancement during the period of the VHE activity. Instead, we detected a factor of ~ 2 decrease in the 0.1-100 GeV flux in 6-month intervals before and after the March 2012 VHE event, suggesting a state change also in the HE regime.

4. By combining the independent measurements of the time-lag in the radio light curves and the core shift between 22 and 43 GHz, we deduced a likely (apparent) speed of the newborn component within the location of the 22-GHz radio core (the physical scale less than 0.1 pc). We derived a sub-relativistic speed of less than $\sim 0.2c$, being consistent with the values reported in previous kinematics measurements in the subparsec region of this jet. On the other hand, the derived speed for the newborn component is significantly slower than that of the component ($\sim 1.1c$) that appeared during the VHE event in 2008. Considering the 2008 VHE activity to be more powerful than the case in 2012, this implies that the stronger VHE activity can be associated with the production of the higher Lorentz factor jet.

We thank the anonymous referee for his/her review and suggestions for improving the paper. We are grateful to E. Torresi for reading and helpful comments on the manuscript. The VERA is operated by Mizusawa VLBI Observatory, a branch of National Astronomical Observatory of Japan. K.H. thanks K. M. Shibata, T. Jike and all of the rest of the staff who helped with operations of the VERA observations presented in this paper. K.H. is supported by the Japan Society for the Promotion of Science (JSPS) Research Fellowship Program for Young Scientists. Part of this work was done with the contribution of the Italian Ministry of Foreign Affairs and University and Research for the collaboration project between Italy and Japan. This work was partially supported by KAKENHI (24340042, 24540240, 24540242, 25120007 and 26800109). e-VLBI research infrastructure in Europe is supported by the European Union's Seventh Framework Programme (FP7/2007-2013) under grant agreement no. RI-261525 NEXPReS. The European VLBI Network is a joint facility of European, Chinese, South African and other radio astronomy institutes funded by their national research councils. The Submillimeter Array is a joint project between the Smithsonian Astrophysical Observatory and the Academia Sinica Institute of Astronomy and Astrophysics and is funded by the Smithsonian Institution and the Academia Sinica.

The *Fermi* LAT Collaboration acknowledges generous ongoing support from a number of agencies and institutes that have supported both the development and the operation of the LAT as well as scientific data analysis. These include the National Aeronautics and Space Administration and the Department of Energy in the United States, the Commissariat à l'Energie Atomique and

the Centre National de la Recherche Scientifique Institut National de Physique Nucléaire et de Physique des Particules in France, the Agenzia Spaziale Italiana and the Istituto Nazionale di Fisica Nucleare in Italy, the Ministry of Education, Culture, Sports, Science and Technology (MEXT), High Energy Accelerator Research Organization (KEK) and Japan Aerospace Exploration Agency (JAXA) in Japan, and the K. A. Wallenberg Foundation, the Swedish Research Council and the Swedish National Space Board in Sweden.

Additional support for science analysis during the operations phase is gratefully acknowledged from the Istituto Nazionale di Astrofisica in Italy and the Centre National d'Études Spatiales in France.

REFERENCES

Abdo, A. A., Ackermann, M., Ajello, M., et al. 2009, ApJ, 707, 55

Abdo, A. A., Ackermann, M., Ajello, M., et al. 2010, ApJ, 719, 1433

Abramowski, A., Acero, F., Aharonian, F., et al. 2012, ApJ, 746, 151

Acciari, V. A., Aliu, E., Arlen, T., et al. 2009, Science, 325, 444

Aharonian, F., Akhperjanian, A. G., Bazer-Bachi, A. R., et al. 2006, Science, 314, 1424

Aliu, E., Arlen, T., Aune, T., et al. 2012, ApJ, 746, 141

Asada, N. & Nakamura, M. 2012, ApJ, 745, L28

Atwood, W. B., Abdo, A. A., Ackermann, M., et al. 2009, ApJ, 697, 1071

Barkov, M. V., Aharonian, F, A., & Bosch-Ramon, V. 2010, ApJ, 724, 1517

Beilicke, M., & VERITAS Collaboration 2012, arXiv:1210.7830

Biretta, J. A., Sparks, W, B., & Macchetto, F. 1999, ApJ, 520, 621

Blakeslee, J. P., Jordán, A., Mei, S., et al. 2009, ApJ, 694, 556

Blandford, R. D., & Königl, A. 1979, ApJ, 232, 34

Brodatzki, K. A., Pardy, D. J. S., Becker, J. K., & Schlickeiser, R. 2011, ApJ, 736, 98

Cheung, C. C., Harris, D. E., & Stawarz, Ł. 2007, ApJ, 663, L65

Chiaberge, M., Capetti, A., Celotti, A. 2001, MNRAS, 324, L33

Dodson, R., Edwards, P. G., & Hirabayashi, H. 2012, PASJ, 58, 243

Doeleman, S. S., Fish, V. L., Schenck, D. E., et al. 2012, Science, 338, 355

Ford, H. C., Harms, R. J., Tsvetanov, Z. I., et al. 1994, ApJ, 435, 27

Gebhardt, K., & Thomas, J. 2009, ApJ, 700, 1690

Gebhardt, K., Adams, J., Richstone, D., Lauer, T. R., Faber, S. M., 2011, ApJ, 729, 119

Georganopoulos, M., Perlman, E. S., & Kazanas, D. 2005, ApJ, 634, L33

Giannios, D., Uzdensky, D. A., & Begelman, M. C. 2010, MNRAS, 402, 1649

Giovannini, G., Cotton, W. D., Feretti, L., Lara, L., & Venturi, T. 2001, ApJ, 552, 508

Giovannini, G., Casadio, C., Giroletti, M., et al. 2011, in ASP Conf. Ser., Vol. 275, Jets at all Scales, eds. G. E. Romero, R. A. Sunyaev & T. Belloni (San Francisco: ASP), 150

Giroletti, M., Hada, K., Giovannini, G., et al. 2012, A&A, 538, L10

Gurwell, M. A., Peck, A. B., Hostler, S. R., Darrah, M. R., & Katz, C. A. 2007, in ASP Conf. Ser., Vol. 375, From Z-Machines to ALMA: (Sub)millimeter Spectroscopy of Galaxies, eds. A. J. Baker, J. Glenn, A. I. Harris, J. G. Mangum & M. S. Yun (San Francisco: ASP), 234

Hada, K., Doi, A., Kino, M., et al. 2011, Nature, 477, 185

Hada, K., Kino, M., Nagai, H., et al. 2012, ApJ, 760, 52

Hada, K., Kino, M., Doi, A., et al. 2013, ApJ, 775, 70

Hada, K. 2013, The Innermost Regions of Relativistic Jets and Their Magnetic Fields, Granada, Spain, Edited by Jose L. Gomez; EPJ Web of Conferences, European Physical Journal Web of Conferences, 61, 1002

Harms, R. J., Ford, H. C, Tsvetanov, Z. I., et al. 1994, ApJ, 435, 35

Harris, D. E., Cheung C. C., Biretta, J. A., et al. 2006, ApJ, 640, 211

Harris, D. E., Cheung, C. C., Stawarz, L., et al. 2008, in ASP Conf. Ser., Vol. 386, Extragalactic Jets: Theory and Observation from Radio to Gamma Ray, ed. T. A. Rector & D. S. De Young (San Francisco: ASP), 80

Harris, D. E., Cheung, C. C., Stawarz, Ł., Biretta, J. A., & Perlman, E. S. 2009, ApJ, 699, 305

Harris, D. E., Massaro, F., Cheung, C. C., et al. 2011, ApJ, 743, 177

Hirota, T., Bushimata, T., Choi, Y.- K., Honma, M., & Imai, H. et al. 2007, PASJ, 59, 897

Honma, M., Bushimata, T., Choi, Y. K., et al. 2007, PASJ, 59, 889

Honma, M., Kijima, M., Suda, H, et al. 2008, PASJ, 60, 935

Junor, W., Biretta, J. A., & Livio, M. 1999, Nature, 401, 891

Komissarov, S. S., Barkov, M. V., Vlahakis, N., & Königl, A. 2007, MNRAS, 380, 51

Königl, A. 1981, ApJ, 243, 700

Kovalev, Y. Y., Lister, M. L., Homan, D. C, & Kellermann, K. I. 2007, ApJ, 668, L27

Kovalev, Y. Y., Lobanov, A. P., Pushkarev, A. B., & Zensus, J. A. 2008, A&A, 483, 759

Krichbaum, T. P., Graham, D. A., Bremer, M., et al. 2006, JPhCS, 54, 328

Kudryavtseva, N. A., Gabuzda, D. C., Aller, M. F., & Aller, H. D. 2011, MNRAS, 415, 1631

Lee, S.-S., Petrov, L., Byun, D.-Y., et al. 2014, AJ, 147, 77

Lenain, J.-P., Boisson, C., Sol, H., & Katarzyński, K. 2008, A&A, 478, 111

Levinson, A., & Rieger, F. 2011, ApJ, 730, 123

Lobanov, A. P. 1998, A&A, 330, 79

Ly, C., Walker, R. C., & Wrobel, J. M. 2004, AJ, 127, 119

Ly, C., Walker, R. C., & Junor, W. 2007, ApJ, 660, 200

Macchetto, F., Marconi, A., Axon, D. J., et al. 1997, ApJ, 489, 579

MAGIC Collaboration, Aleksić,, J., Ansoldi, S., et al. 2013, arXiv:1310.8500

Marscher, A. P., & Gear, W. K. 1985, ApJ, 298, 114

Marscher, A. P., Jorstad, S. G., D'Arcangelo, F. D., et al. 2008, Nature, 452, 966

Mattox, J. R., Bertsch, D. L., Chiang, J., et al. 1996, ApJ, 461, 396

McKinney, J. C. 2006, MNRAS, 368, 1561

Nagai, H., Kino, M., Niinuma, K, et al. 2013, PASJ, 65, 24

Nagai, H., Haga, T., Giovannini, G, et al. 2014, ApJ in press

Neronov, A., & Aharonian, F. A. 2007, ApJ, 671, 85

Nolan, P., Abdo, A. A., Ackermann, M., et al. 2012, ApJS, 199, 31

Orienti, M., Koyama, S., D'Ammando, F., et al. 2013, MNRAS, 428, 2418

Owen, F. N., Hardee, P. E., & Cornwell, T. J. 1989, ApJ, 340, 698

Perlman, E. S., Biretta, J. A., Sparks, W. B., Macchetto, F. D., & Leahy, J. P. 2001, ApJ, 551, 206

Perlman, E. S., Adams, S. C., Cara, M., et al. 2011, ApJ, 743, 119

Reid, M. J., Biretta, J. A., Junor, W., Muxlow, T. W. B., & Spencer, R. E. 1989, ApJ, 336, 112

Reimer, A., Protheroe, R. J., & Donea, A.-C. 2004, A&A, 419, 89

Rieger, F. M., & Aharonian, F. A. 2008, A&A, 479, L5

Reynoso, M. M., Medina, M. C., & Romero, G. E. 2011, A&A 531, 30

Sawada-Satoh, S. 2013, The proceedings of the 11th Asian-Pacific Regional IAU Meeting, 1, 538

Stawarz, Ł., Aharonian, F., Kataoka, J., et al. 2006, MNRAS, 370, 981

Tavecchio, F., & Ghisellini, G. 2008, MNRAS, 385, L98

Urry, C. M., Padovani, P. 1995, PASP, 107, 803

Valtaoja, E., Terasranta, H., Urpo, S., et al. 1992, A&A, 254, 71

Walsh, J. L., Barth, A. J., Ho, L. C., & Sarzi, M. 2013, ApJ, 770, 86

This preprint was prepared with the AAS LaTeX macros v5.2.